

# Space Filling Curves is All You Need: Communication-Avoiding Matrix Multiplication Made Simple

Evangelos Georganas, Alexander Heinecke, Pradeep Dubey  
Intel Corporation

**Abstract**—General Matrix Multiplication (GEMM) is the cornerstone of Deep Learning and HPC workloads; accordingly, academia and industry have heavily optimized this kernel. Modern platforms with matrix multiplication accelerators exhibit high FLOP/Byte machine balance, which makes implementing optimal matrix multiplication challenging. On modern CPU platforms with matrix engines, state-of-the-art vendor libraries tune input tensor layouts, parallelization schemes, and cache blocking to minimize data movement across the memory hierarchy and maximize throughput. However, the best settings for these parameters depend strongly on the target platform (number of cores, memory hierarchy, cache sizes) and on the shapes of the matrices, making exhaustive tuning infeasible; in practice this leads to performance “glass jaws”. In this work we revisit space filling curves (SFC) to alleviate the problem of this cumbersome tuning. SFC convert multi-dimensional coordinates (e.g. 2D) into a single dimension (1D), keeping nearby points in the high-dimensional space close in the 1D order. We partition the Matrix Multiplication computation space using recent advancements in generalized SFC (Generalized Hilbert Curves), and we obtain platform-oblivious and shape-oblivious matrix-multiplication schemes that exhibit inherently high degree of data locality. Furthermore, we extend the SFC-based work partitioning to implement Communication-Avoiding (CA) algorithms that replicate the input tensors and provably minimize communication/data-movement on the critical path. The integration of CA-algorithms is seamless and yields compact code (~30 LOC), yet it achieves state-of-the-art results on multiple CPU platforms, outperforming vendor libraries by up to 2× (geometric-mean speedup) for a range of GEMM shapes.

## I. INTRODUCTION

Deep Learning (DL) has brought significant advancements in various fields, including computer vision, natural language processing, recommender systems, and even traditional scientific domains [1]–[10]. Despite the apparent differences between conventional High Performance Computing (HPC) and DL workloads, the computational kernels used in both fields largely overlap, with tensor contractions (dense and sparse) being the most prominent motif [11], [12].

The cornerstone of the time-consuming tensor contractions is General Matrix Multiplication (GEMM), thus academia and industry have optimized this kernel for decades. Modern platforms with matrix multiplication accelerators exhibit high FLOP/byte machine balance, making optimal matrix multiplication implementation a challenge. For modern CPU platforms with matrix engines, state-of-the-art vendor libraries optimize the input tensor layouts, the parallelization schemes and the cache-blocking in order to minimize data-movement across the memory hierarchy and optimize throughput. However, the optimal tunings for the aforementioned parameters highly depend on the platform at hand (number of cores, memory hierarchy, cache-sizes) as well as the shapes of the involved matrices,

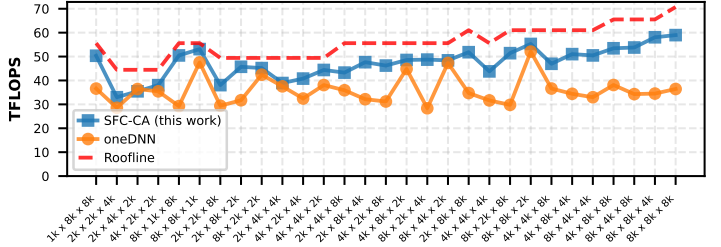


Fig. 1: Multi-core GEMM performance (Bfloat16) of a vendor-optimized library (oneDNN) and this work (SFC-CA) on a platform with Matrix Multiplication Accelerator (64-core Intel Xeon Emerald Rapids). The x-axis shows the  $M \times N \times K$  GEMM configurations. OneDNN illustrates performance “glass jaws” and is far-off the roofline.

making the optimal tuning of these libraries infeasible, and in practice this translates to performance “glass jaws”. For example, in Figure 1 we illustrate with orange color the multi-core GEMM performance (Bfloat16 precision) of a vendor-optimized library (oneDNN) on a platform with Matrix Multiplication Accelerator (64-core Intel Xeon Emerald Rapids with Advanced Matrix Extensions). The vendor-optimized library illustrates performance “glass jaws” and is far-off the roofline performance even for shapes with large operational intensity.

To tackle the cumbersome tuning of GEMM implementations, recent work [13] (namely PARLOOPPER) introduced a framework to develop efficient, portable GEMM kernels for modern CPU architectures by decomposing the kernel development in two steps: 1) Expressing the computational core using Tensor Processing Primitives (TPPs) [12]: a compact, versatile set of 2D-tensor operators, 2) Expressing the logical loops around TPPs in a high-level, declarative fashion whereas the exact instantiation (ordering, tiling, parallelization) is determined via simple knobs. In the specific case for GEMM kernels, PARLOOPPER uses the Batch-Reduce GEMM (BRGEMM) TPP [14] to address the code generation problem of the core computation kernel (i.e. single-core tensor contraction). To address the problem of generating arbitrarily complex parallel loops around the single-core BRGEMM TPP, PARLOOPPER simplifies the “outer loop” writing by enabling the user to declare the logical “outer loops” along with their specifications (i.e. bounds/steps/parallelization properties), instead of explicitly writing the tedious loop nests that pertain to multiple loop orders, tilings and parallelization schemes. At runtime, the user may provide a single knob/parameter to dictate the desired instantiation of the loop nest (i.e. loop order, loop blockings/tilings, parallelization method). Even

though PARLOOPER simplifies the overall development effort for optimal GEMM kernels, eventually finding the “value” of the single knob that maximizes the performance for the platform and GEMM problem at hand requires expensive/time-consuming platform-specific auto-tuning, or some heuristics for deriving “sufficiently good” knob values (although the heuristic-derived knob might yield suboptimal performance).

In this work we revisit space filling curves (SFC) to alleviate the problem of this convoluted outer-loop tuning. SFC convert multi-dimensional coordinates (e.g. 2D) into a single dimension (1D), keeping nearby points in the high-dimensional space close in the 1D order. We partition the Matrix Multiplication computation space using recent advancements in generalized space filling curves (Generalized Hilbert Curves [15]), and we obtain platform-oblivious and shape-oblivious matrix-multiplication schemes that exhibit inherently high degree of data locality. Unlike previous work [16] that used SFC to determine locality-friendly tensor layouts, but fails to generalize, yields complicated indexing in the micro-kernels and eventually offers limited performance upside over vendor-optimized libraries, we merely use the SFC to partition the *tiled* GEMM computation space and we use the BRGEMM TPP for optimal single-core/single-output tensor tile code generation. Furthermore, we extend the SFC-based work partitioning to implement Communication-Avoiding (CA) 2.5D GEMM algorithms that replicate the input tensors and provably minimize communication/data-movement on the critical path of execution [17], [18]. The integration of the 2.5D CA-algorithms with the SFC-based partitioning is seamless and yields compact code ( $\sim 30$  LOC), yet it achieves state-of-the-art (SOTA) results on multiple CPU platforms (x86 and Arm), outperforming vendor-optimized libraries by up to  $2\times$  (geometric-mean speedup) across a range of GEMM shapes with varying aspect ratios. The contributions of this work are:

- A SFC-based, Communication-Avoiding (SFC-CA) Matrix Multiplication algorithm that leverages the BRGEMM TPP as building block for the single-core/thread-local tensor contraction code generation. SFC-CA GEMM obviates the need for outer loop tuning, is inherently platform-oblivious (i.e. memory hierarchy, number of cores, cache sizes) and GEMM-shape-oblivious, and provably minimizes communication (i.e. data movement from memory/last-level cache to private L2 cache) along the critical path of execution. As a result, the same compact implementation ( $\sim 30$  C++ LOC) outperforms consistently vendor-optimized GEMM libraries across a range of GEMM shapes and CPU platforms.
- Detailed GEMM benchmarking across various contemporary CPU platforms (x86 and Arm/Aarch64), illustrating portable, State-Of-The-Art (SOTA) performance that outperforms optimized libraries by up to  $2\times$  (geometric-mean speedup). We analyze the obtained performance by devising tight roofline performance models and illustrate that the SFC-CA GEMM closely tracks the roofline.



Fig. 2: SFC-based traversal of  $16\times 16$  grid. The SFC used is the generalized 2D Hilbert curve. The numbers in the grid boxes indicate the order (i.e. timestamp) of the traversal, also color-coded according to the heatmap bar on the right.

## II. SFC-BASED COMMUNICATION-AVOIDING GEMM

### A. Generalized Hilbert SFC

The discrete Hilbert curve is a widely used space-filling curve to map between  $N$ -dimensional and 1-D spaces while preserving locality. However, classical algorithms only work for domains whose sides are powers of two. Recent work [15] presents a simple recursive algorithm that generalizes the Hilbert curve to rectangles of arbitrary sizes in 2D (henceforth this work refers to this generalized Hilbert curve as SFC for brevity). Hilbert curves split a finite 2D space into recursive quadrants and traverse each quadrant in recursive “U” shapes at each iteration such that every quadrant gets fully visited before moving onto the next one.

Figure 2 illustrates SFC-based traversal of a  $16\times 16$  grid. The SFC used is the generalized 2D Hilbert curve. The numbers in the grid boxes indicate the order (i.e. timestamp) of the grid traversal, also color-coded according to the heatmap bar. We make two key observations that inspire our SFC-CA GEMM outlined in Section II-D. First, we observe that adjacent 1D SFC indices lie in neighboring boxes in the 2D space (i.e. there are no “big jumps” in the 2D space as we march along the 1D SFC index). Second, due to the recursive nature of the SFC, the grid is partitioned in a locality-aware fashion by selecting continuous ranges of indices in the 1D SFC space. For example, by selecting the boxes with 1D indices 0 - 31 we get a contiguous  $8\times 4$  2D rectangular “patch” from the original  $16\times 16$  2D grid (top-left). Also, the subset of 1D indices 8-15 yields yet another contiguous  $2\times 4$  2D rectangular “sub-patch” within the aforementioned  $8\times 4$  rectangular “patch”.

### B. 2.5D Communication-Avoiding GEMM Algorithm

In a distributed memory setup, the 2.5D Communication-Avoiding GEMM algorithm [17], [18] is an extension of

classic 2D algorithms (like Cannon’s or SUMMA) designed to reduce communication costs by utilizing available extra memory to replicate data.

For the matrix multiplication  $C = A \times B$ , where matrices are of size  $n \times n$ , the  $P$  processors are organized into a 3D logical grid of size  $\sqrt{P}/c \times \sqrt{P}/c \times c$ , where  $c$  is the replication factor ( $1 \leq c \leq P^{1/3}$ ). The input matrices are replicated, with one copy of  $C$  distributed across each of the  $c$  layers of the processor grid. Each layer performs a  $1/c$  fraction of the total work (sum of outer products) independently by having each layer of processors working effectively on  $A$  and  $B$  panels with logical inner-product dimension  $K/c$ . A final reduction step is performed across the  $c$  layers to aggregate partial results into the final matrix  $C$ .

The 2.5D algorithm achieves the following communication costs per processor for bandwidth  $W$  (words moved), latency  $L$  (number of messages) and memory usage  $M$ :  $W = O\left(\frac{n^2}{\sqrt{c}P}\right)$ ,  $L = O\left(\sqrt{\frac{P}{c^3}} + \log c\right)$  and  $M = O\left(\frac{cn^2}{P}\right)$ . When  $c = 1$ , the algorithm matches the 2D lower bound. As  $c$  increases toward  $P^{1/3}$ , the bandwidth cost is reduced by a factor of  $\sqrt{c}$ , effectively trading surplus memory for reduced communication volume on the critical path. For the rest of the paper and since we are considering the use-case of shared-memory parallel matrix multiplication, we are focusing on the lower bounds in communication pertaining in number of words moved. The number of messages is proportional to the number of words, since in the shared memory systems the “message” size equals to the cache-line size. Therefore, an algorithm minimizing the number of words moved on the critical path minimizes simultaneously the number of messages/cache-lines moved across the memory hierarchy.

### C. Tensor Processing Primitives and GEMM notations

In the context of this work, one can think the Tensor Processing Primitives as a set of single threaded/serial microkernels operating on 2D tensor tiles. In principle, given an architecture and tile shape, one can devise an optimal implementation for the TPPs that adopts conventional vectorization and register blocking optimizations. The key point is that these single-core/single-threaded optimizations for the underlying microkernels are abstracted by the TPP abstraction layer and are undertaken by the TPP backend implementation which is platform-specific [12].

We leverage the Tensor Processing Primitives (TPP) [12] as building blocks, and more specifically the TPPs we use are the *zero\_tpp*, the *add\_reduce\_tpp* and the *brgemm\_tpp*. The *zero\_tpp* merely sets the input 2D tensor tile to zero values. The *add\_reduce\_tpp* accumulates multiple 2D tensor tiles that are separated by a fixed stride. The *brgemm\_tpp* corresponds to the *Batch-Reduce GEMM* (BRGEMM) TPP which is the main building block for general tensor contractions in the TPP collection [12], [14]. BRGEMM materializes the operation  $C = \beta \cdot C + \sum_{i=0}^{brcount-1} A_i \times B_i$ . This kernel multiplies the specified blocks  $A_i^{bm \times bk}$  and  $B_i^{bk \times bn}$  and reduces the partial results to a block  $C^{bm \times bn}$ . In this work we use the *stride-based* variant of BRGEMM, where the addresses of  $A_i$

### Listing 1 SFC-based Communication-Avoiding GEMM

```

1  Dtype A[Mb][Kb][bk][bm]; //Block M with bm and K with bk
2  Dtype B[Nb][Kb][bn][bk]; //Block N with bn and K with bk
3  Dtype C[K_layers][Nb][Mb][bn][bm]; //Block N with bn and M with bm
4
5  sfc_map = create_sfc_map(Mb, Nb);
6  Kb_per_layer = Kb / K_layers;
7  Kb_per_brgemm = Kb_per_layer / k_block_factor;
8
9  for (ik = 0; ik < k_block_factor; ik++) { //K-block for A/B panel-size
10 #pragma omp parallel for
11   for (i = 0; i < Mb * Nb * K_layers; i++) {
12     i_layer = i / (Mb * Nb); // Index for K_layer
13     i_sfc = i % (Mb * Nb); // ID index for SFC within K-layer
14     (im, in) = map_sfc_index(sfc_map, i_sfc); //ID SFC index -> im, in
15     //Extract k_block_index based on K-layer (i_layer) & ik K-block
16     k_block_index = i_layer * Kb_per_layer + ik * Kb_per_brgemm;
17     if (ik == 0) zero_tpp(&C[i_layer][in][im][0][0]); //Zero C block
18     // Execute tensor contraction with A/B panels on proper C block
19     brgemm_tpp(&A[im][k_block_index][0][0],
20                &B[in][k_block_index][0][0],
21                &C[i_layer][in][im][0][0], &Kb_per_brgemm );
22   }
23 }
24
25 // Reduce C matrices across K layers
26 if (K_layers > 1) {
27 #pragma omp parallel for
28   for (i = 0; i < Mb * Nb; i++) {
29     in = i % Nb;
30     im = i / Nb;
31     reduce_stride = M * N;
32     C_block_final = &C[0][in][im][0][0];
33     add_reduce_tpp(C_block_final, K_layers, reduce_stride);
34   }
35 }

```

and  $B_i$  are:  $address\_A_i = address\_A_{i-1} + stride\_A$  and  $address\_B_i = address\_B_{i-1} + stride\_B$  [12].

The Matrix Multiplication input tensors are logically 2D matrices  $A^{M \times K}$  and  $B^{K \times N}$  that need to be multiplied and added onto  $C^{M \times N}$ . To maximize performance, we follow the approach of previous work [14] and we block the dimensions  $M$ ,  $K$ , and  $N$  by factors  $bm$ ,  $bk$ , and  $bn$  respectively (lines 1-3 of Listing 1). We employ the BRGEMM TPP to perform the tensor contraction with  $A$  and  $B$  across their dimensions  $Kb$  and  $bk$  (which constitute the  $K$ /inner-product dimension of the original 2D matrices). In regard to the stride-based BRGEMM setup, the sub-blocks  $A_i$  and  $B_i$  that have to be multiplied and reduced are apart by fixed strides  $stride\_A = bk \cdot bm$  and  $stride\_B = bn \cdot bk$ .

### D. SFC-Based Communication-Avoiding GEMM Algorithm

Listing 1 illustrates the pseudocode of our SFC-Based Communication-Avoiding shared-memory GEMM Algorithm. As mentioned earlier, we block the dimensions  $M$ ,  $K$ , and  $N$  by factors  $bm$ ,  $bk$ , and  $bn$  respectively (lines 1-3 of Listing 1). Consequently, the GEMM computation space consists of  $Mb \times Nb$  output  $C$  tiles with  $Mb = M/bm$  and  $Nb = N/bn$ . Then, we create the SFC corresponding to this 2D  $Mb \times Nb$  grid (line 5). Also, we have a tunable parameter  $K\_layers$  that effectively partitions the global  $K$  dimension by this factor  $K\_layers$  and determines the number of copies of  $C$  matrix (observe the outer dimension of  $C$  in line 3 is  $K\_layers$ ). Each one of the  $C$  copies will be computed by the corresponding distinct  $K$ -partition of  $A$  and  $B$  tensors. Finally we also pick a blocking factor for the logical  $K$  dimension ( $k\_block\_factor$ ) which is merely controlling the sub-panel sizes of  $A$  and  $B$  tensors within each  $K$ -partition (this is effectively the loop in line 9).

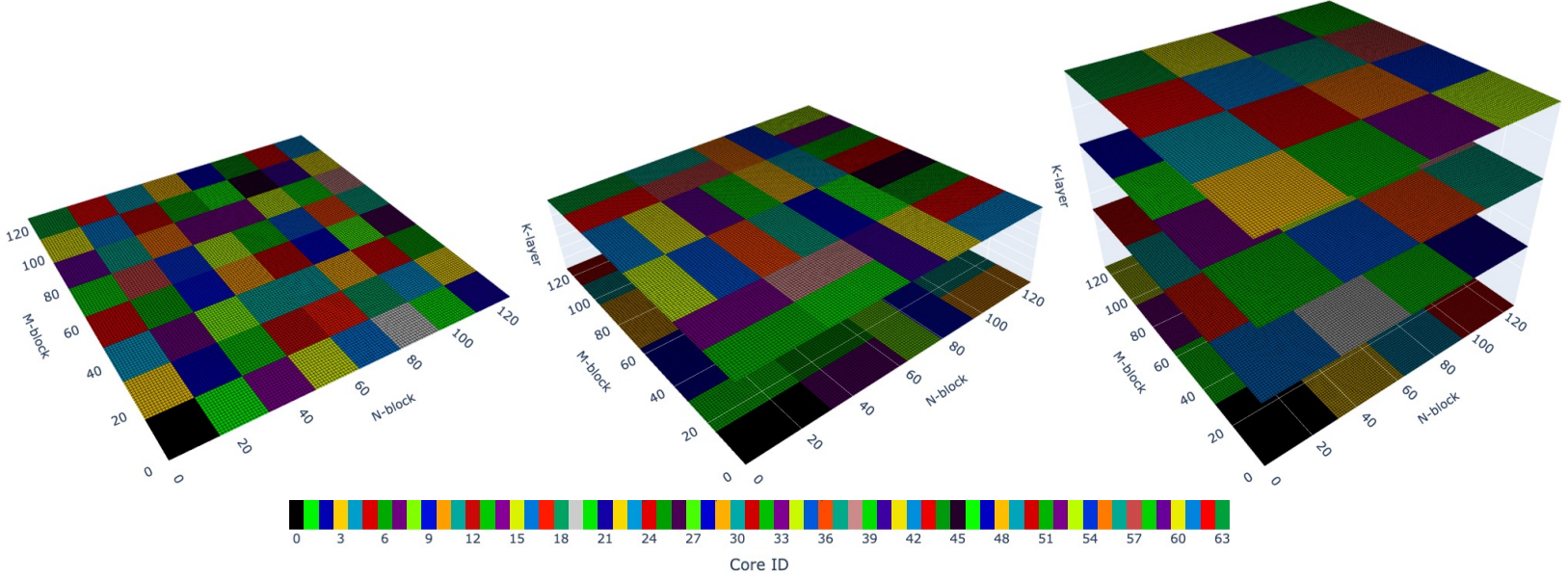


Fig. 3: SFC-based partitioning of  $C$  matrix using 64 cores. The  $C$  dimensions are  $4096 \times 4096$ , and by using blocks of size  $32 \times 32$  we obtain a grid of  $128 \times 128$   $C$  blocks. **Left:** 2D  $C$  decomposition, the SFC yields a 2D core decomposition (grid of  $8 \times 8$  cores). Each core is implicitly assigned a  $C$  tile consisting of  $16 \times 16$   $C$  blocks (each having size  $32 \times 32$ ). Each core-local grid of  $16 \times 16$   $C$  blocks/ $C$ -tasks is traversed by the core using the SFC ordering illustrated in Figure 2. **Middle:** 2.5D decomposition by replicating  $C$  by a factor of 2 (i.e. 2 layers of  $C$ ), within each layer the SFC yields a 2D core decomposition with rectangular  $C$  tiles. Within each layer of  $C$  the work is partitioned among 32 cores. **Right:** 3D decomposition of  $C$  by replicating it by a factor of 4. Within each layer the SFC yields a 2D core decomposition ( $4 \times 4$  core decomposition within each plane), for a logical  $4 \times 4 \times 4$  3D grid of cores.

The interesting loop which constitutes the heart of our GEMM algorithm is the one in line 11. Effectively we create a “task iteration space” with size  $Mb \times Nb \times K\_layers$  and we assign with a simple `#pragma omp parallel for` these iterations to the available  $T$  cores/threads in a block fashion. Using the modulo logic in lines 12-13 we *implicitly* map the first  $Mb \times Nb$  work-items (corresponding to the first  $C$  layer) to the first “team” of  $T/K\_layers$  cores, the second batch of  $Mb \times Nb$  work-items to the second “team” of  $T/K\_layers$  cores etc. If we have  $K\_layers = 1$  then we just have 1  $C$  copy and just 1 team of  $T$  cores. With the same modulo logic, we assign again *implicitly* the contiguous 1D indices from the range  $0 \dots Mb \times Nb - 1$  to the  $T/K\_layers$  cores of that corresponding team. By leveraging the precomputed SFC map, we map each thread-specific  $i\_sfc$  1D SFC-index to the proper  $im$  and  $in$  block of the  $C$  matrix copy/layer that this thread/core will be working on (line 14). Next, with a BRGEMM TPP we perform the corresponding contraction on the  $im$  and  $in$  block of the  $C$  matrix copy by using the proper panels of  $A$  and  $B$  (lines 19-21). Finally, if we have  $K\_layers > 1$ , we perform a reduction among the  $K\_layers$  of  $C$  copies since each  $C$  copy on each  $K$ -layer holds only a partially computed contraction (lines 26-35).

This very simple algorithm, yields effectively a class of GEMM decompositions that can be seen in Figure 3. For  $K\_layers = 1$  we get a traditional 2D GEMM decom-

position (recall the observations from Section II-A), and for  $K\_layers > 1$  we get effectively the Communication-Avoiding 2.5D and 3D GEMM decompositions [17], [18]. More specifically, in Figure 3 we illustrate the SFC-based partitioning of a  $C$  matrix using  $T = 64$  cores. The  $C$  dimensions are  $4096 \times 4096$ , and by using blocks of size  $32 \times 32$  ( $bm = bn = 32$ ) we obtain a grid of  $128 \times 128$  output  $C$  blocks. In Figure 3-Left we illustrate a 2D  $C$  decomposition ( $K\_layers = 1$ ): the SFC yields *implicitly* a 2D core decomposition (grid of  $8 \times 8$  cores). Each core is implicitly assigned a  $C$  tile/“patch” consisting of  $16 \times 16$   $C$  output blocks (each having size  $32 \times 32$ ). Each core-local grid of  $16 \times 16$   $C$  blocks/ $C$ -tasks is traversed by the core using the SFC ordering illustrated in Figure 2, and inherently exhibits temporal and spatial locality, obviating the need for explicit cache-blocking and loop reordering. In Figure 3-Middle we illustrate a 2.5D decomposition: by replicating  $C$  by a factor of 2 (i.e.  $K\_layers = 2$ ), within each layer the SFC yields *implicitly* a 2D core decomposition with rectangular  $C$  tiles. Within each layer of  $C$  the work is partitioned among 32 cores. Finally in Figure 3-Right we illustrate a 3D decomposition of  $C$  by replicating it by a factor of 4. Within each layer the SFC yields *implicitly* a 2D core decomposition ( $4 \times 4$  core decomposition within each plane), for a logical  $4 \times 4 \times 4$  3D grid of cores. We emphasize that all these decompositions happen *implicitly* by leveraging the SFC properties and the

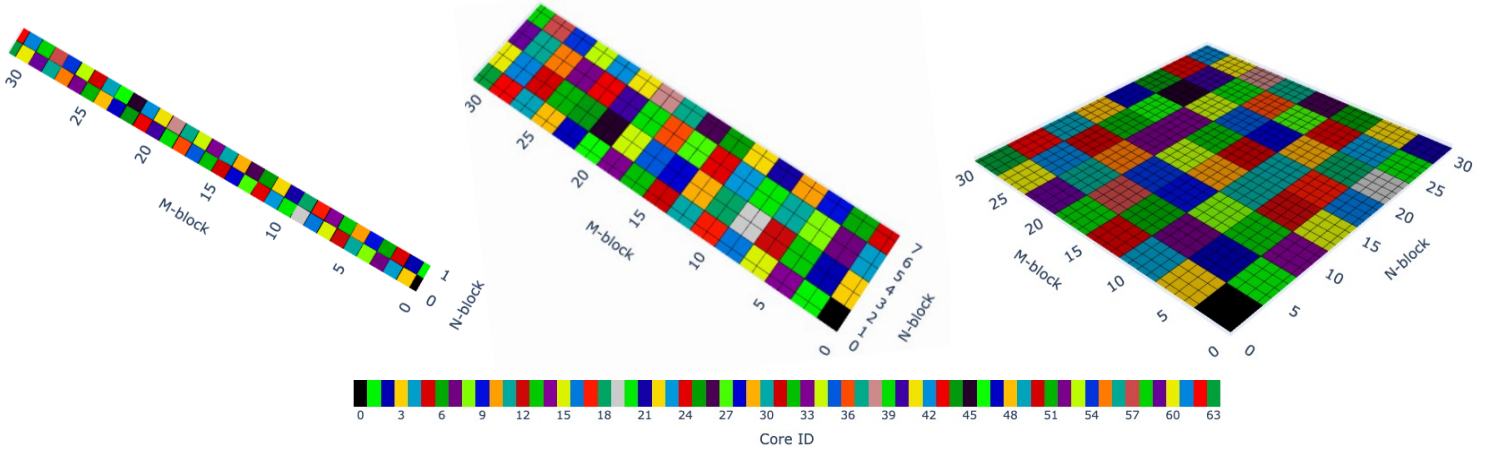


Fig. 4: SFC-based partitioning of  $C$  matrices with different  $M:N$  aspect ratios using 64 cores. The SFC-based partitioning yields 2D core decompositions with aspect ratios matching the corresponding  $M:N$  ratio.

proper loop-index mapping in lines 12-14.

#### E. Communication optimality of SFC-CA GEMM Algorithm

In this subsection we sketch out how our SFC-CA GEMM algorithm achieves asymptotically the lower bound mentioned in subsection II-B. For this shared-memory analysis, we will use the following simplified performance model: Each core in a system with  $T$  total cores has access to *fast memory* (i.e. L2 cache) with size *FastMem*, and all the reads/writes from/to this fast memory are essentially “free”, considering that the reads/writes from/to main memory (or last level shared cache) are 1-2 orders of magnitude slower (henceforth we refer to main memory/last level shared cache as *slow memory*).

Before diving into the communication/data-movement analysis of the SFC-CA GEMM algorithm, it is important to highlight the thread decompositions that organically arise by using SFC-based work partitioning. Due to the fact that Hilbert curves split a finite 2D space into recursive quadrants and traverse each quadrant recursively such that every quadrant gets fully visited before moving onto the next one, the thread decompositions that partition the 1D SFC-index space in a block fashion naturally result in thread grids with aspect ratios matching the aspect ratios of the partitioned 2D space. In Figure 4 we illustrate SFC-based partitioning of  $C$  matrices with different  $M:N$  aspect ratios using 64 cores. The SFC-based partitioning yields 2D core decompositions with aspect ratios matching the corresponding  $M:N$  ratio. In Figure 4-Left we see a  $C$  matrix with aspect ratio  $M:N = 16:1$  and the resulting thread decomposition is a logical  $32 \times 2$  grid, which also has aspect ratio  $16:1$ . In Figure 4-Middle exhibits a  $C$  matrix with aspect ratio  $M:N = 4:1$  and the resulting thread decomposition is a logical  $16 \times 4$  grid, which also has aspect ratio  $4:1$ . Finally, Figure 4-Right illustrates a square  $C$  matrix with aspect ratio  $M:N = 1:1$  and the resulting thread decomposition is a logical square  $8 \times 8$  grid, which also has aspect ratio  $1:1$ .

First we focus on the case with square matrices, i.e.  $M = N = K = n$ . Under these assumptions, we will prove

that our SFC-CA GEMM achieves the lower bounds per core mentioned in subsection II-B. Assume now that each core has sufficiently large fast memory with size *FastMem* to hold  $\Theta(c \cdot n^2/T + 2 \cdot n/(\sqrt{T}/c))$  entries where  $c$  is the replication factor and  $c = K_{\text{layers}}$  in our notation (e.g. in Figure 3). Based on the observation of the previous paragraph, the cores are forming a logical  $\sqrt{T}/c \times \sqrt{T}/c \times c$  logical grid, thus we get on each layer of output  $C$  matrix the same square 2D thread decomposition as the 2.5D GEMM algorithm [17] (see Figure 3-Right).

Each core first allocates and persistently stores its assigned part of matrix  $C$  that is responsible to compute in its local *fast* memory. This local chunk of  $C$  copy has size  $\Theta(c \cdot n^2/T)$  thus per definition fits in the fast memory of size *FastMem*. Then, each core reads from slow memory (memory or shared last level cache) a column of  $A$  with size  $\Theta(n/(\sqrt{T}/c) \times 1)$ , a row of  $B$  with size  $\Theta(1 \times n/(\sqrt{T}/c))$  and maximally uses them to compute an outer-product and update its local chunk of  $C$  copy in the fast memory. Note that these  $A$  and  $B$  “vector-slices” are minimally required by e.g. the decomposition shown in Figure 3. Assuming we have more available vacant space in our fast memory, we can hold *panels* of  $A$  and  $B$  with size  $\Theta(n/(\sqrt{T}/c) \times k')$  where  $k'$  is a small configurable constant, and each core can maximally reuse these panels to update its local chunk of  $C$  copy in the fast memory. Either way, in total each core has to read on the critical path  $K/K_{\text{layers}} = n/c$  columns of  $A$  and  $n/c$  rows of  $B$  to fully compute its local part of  $C$ . Therefore, during the GEMM (lines 9-23 in our SFC-CA Algorithm) each core reads from slow memory for the required  $A$  and  $B$  portion  $\Theta(n/(\sqrt{T}/c) \cdot n/c) = \Theta(n^2/\sqrt{T} \cdot c)$  words, which matches the lower bound from subsection II-B (i.e. this is the communication up to line 24 in the algorithm/before the  $C$  reduction). Note also that the *k\_block\_factor* in line 9 essentially controls the small constant  $k'$  introduced earlier. The final  $C$  reduction (lines 26-35) is identical to the one in the original 2.5D algorithm [17] where it is shown it constitutes a low-order term for the words moved on the critical path.

Therefore, our shared-memory SFC-CA GEMM algorithm minimizes the number of words moved from slow memory and it achieves (asymptotically) the lower bound introduced in subsection II-B.

Now we focus on the case of rectangular matrix multiplication. Without loss of generality, we assume  $M \geq N$  (i.e. the cases illustrated in Figure 4). Since we can adjust the parameter  $k\_block\_factor$  of the SFC-CA GEMM to control the sizes of panels  $A$  and  $B$  by blocking the  $K$ /inner-product dimension, we are interested in the cases of “2 large dimensions” and “3 large dimensions” for rectangular matrix multiplication [19]. More specifically, we are interested in the cases with  $M/N < T < MN/K^2$  and  $MN/K^2 < T$ . For these cases, the corresponding asymptotic bandwidth lower bound costs are  $W = O(\sqrt{(K^2 MN)/T})$  and  $W = O((MNK)/(T\sqrt{FastMem}) + ((MNK)/T)^{\frac{2}{3}})$  respectively [19]. By controlling the replication factor  $c$ , our SFC-CA GEMM Algorithm effectively yields a logical  $T_m \times T_n \times c$  thread decomposition where on each layer of  $T_m \times T_n$  threads we partition the  $C$  matrix (per layer) into a 2D rectangular grid of cores, and the resulting algorithm is virtually identical to the 2D/3D SUMMA [20] with stationary  $C$  matrix which achieves the aforementioned bounds [19].

#### F. Performance modeling

In order to assess the efficiency of our SFC-CA GEMM, we devise *fine-grained* roofline models similar to the ones described in prior work [21]. More specifically, we apply the traditional roofline model [22] at the granularity of the BRGEMM level instead of the whole GEMM operation, and in this way we are able to obtain a *tight* roofline bound.

More specifically, in the simplistic model of infinite/ideal fast memory per core, we can distinguish 4 types of BRGEMM invocations in the SFC-CA GEMM: i)  $BRGEMM_0$  where both  $A$  and  $B$  panels are coming from slow memory, ii)  $BRGEMM_1$  where *only* the  $A$  panel is coming from slow memory (the  $B$  panel was used in a previous BRGEMM and as such is resident in fast memory), iii)  $BRGEMM_2$  where *only* the  $B$  panel is coming from the slow memory (the  $A$  panel was used in a previous BRGEMM and as such is resident in fast memory), and iv)  $BRGEMM_3$  where both  $A$  and  $B$  are resident in the *fast* memory because they have been previously used in a BRGEMM by the same core/thread. The key point here is that given a GEMM problem shape and a thread decomposition, we can analytically calculate the types of BRGEMM invocations that arise on the critical path, and we can accurately project the execution time of these BRGEMM invocations by applying roofline first principles. Let us denote: i)  $\gamma$  the inverse compute ratio per core (i.e. cycles per flop) when all the operands of the BRGEMM are resident in fast memory, ii)  $\beta$  the inverse-read bandwidth of the core when reading shared data from slow memory (i.e. cycles per byte), iii)  $G$  the number of floating point computations per BRGEMM, and iv)  $S_A$  and  $S_B$  the panel sizes in bytes of  $A$  and  $B$  required for the BRGEMM. By applying the simple roofline principle and assuming that the BRGEMM  $C$

load/stores are serviced from/to fast memory, we can derive the following models for the various BRGEMM types.

$$Cycles_{BRGEMM_0} = \max(G \cdot \gamma, \beta \cdot (S_A + S_B)) \quad (1)$$

$$Cycles_{BRGEMM_1} = \max(G \cdot \gamma, \beta \cdot S_A) \quad (2)$$

$$Cycles_{BRGEMM_2} = \max(G \cdot \gamma, \beta \cdot S_B) \quad (3)$$

$$Cycles_{BRGEMM_3} = G \cdot \gamma \quad (4)$$

Then we sum up all the cycles calculated for all the BRGEMM types on the critical path, and additionally we include the time to read/write  $C$  from/to last memory (we have to read and write at least once the output  $C$ ). In case we have to perform a final  $C$  reduction (i.e. 2.5D or 3D SFC-CA GEMM) we also include the time for reading/writing the multiple copies of  $C$ .

We constructed a performance model that given a GEMM shape  $M \times N \times K$  and a number of available cores/threads, it iterates over all possible 2D and 3D thread decompositions and calculates the execution time for each configuration given the parameters  $\beta$  and  $\gamma$ , which can be calculated via microbenchmarks (e.g. [23] and [24]). Finally we report as roofline performance the *minimum* execution time across all configurations or equivalently the *maximum* achieved compute throughput.

#### G. Implementation details

We implemented the SFC-CA GEMM algorithm in C++ and the code is virtually identical to Listing 1. Even though here we utilized OpenMP to partition the 1D SFC index space in a block fashion, *any* rudimentary way to partition this index space among threads in a block fashion will have the same effect with respect to the SFC-CA GEMM efficacy. For the TPP building blocks we leveraged the implementation within LIBXSMM [23], which offers optimized machine code generation Just-In-Time (JIT) for x86 and arm/Aarch64 architectures. For the generation of SFC index maps we leveraged the code from recent work that works for arbitrary rectangular domains [15]. Last but not least, note that the precision in the SFC-CA GEMM implementation of Listing 1 may be parameterized, i.e. DType can be Bfloat16, single precision, double precision, FP8 etc. The algorithm/implementation stays the same, and all the precision-specific code generation is undertaken by the TPP abstraction/backend, which emits at runtime (i.e. JIT) optimal machine code for the precision and machine at hand.

### III. RESULTS

#### A. Experimental Platforms and Setup

In order to assess the performance of the SFC-CA GEMM we experimented with a variety of contemporary CPU platforms, which offer a variety of Matrix Multiplication Acceleration engines:

**Emerald Rapids (EMR):** An Intel Xeon Platinum 8592+ CPU with 64 cores and 1024GB DDR5@5600 memory. EMR offers Intel AMX technology for matrix multiplication acceleration [25].

**Granite Rapids (GNR):** An Intel Xeon 6980 CPU with 128 cores and 1536GB DDR5@8800. GNR also offers Intel AMX technology.

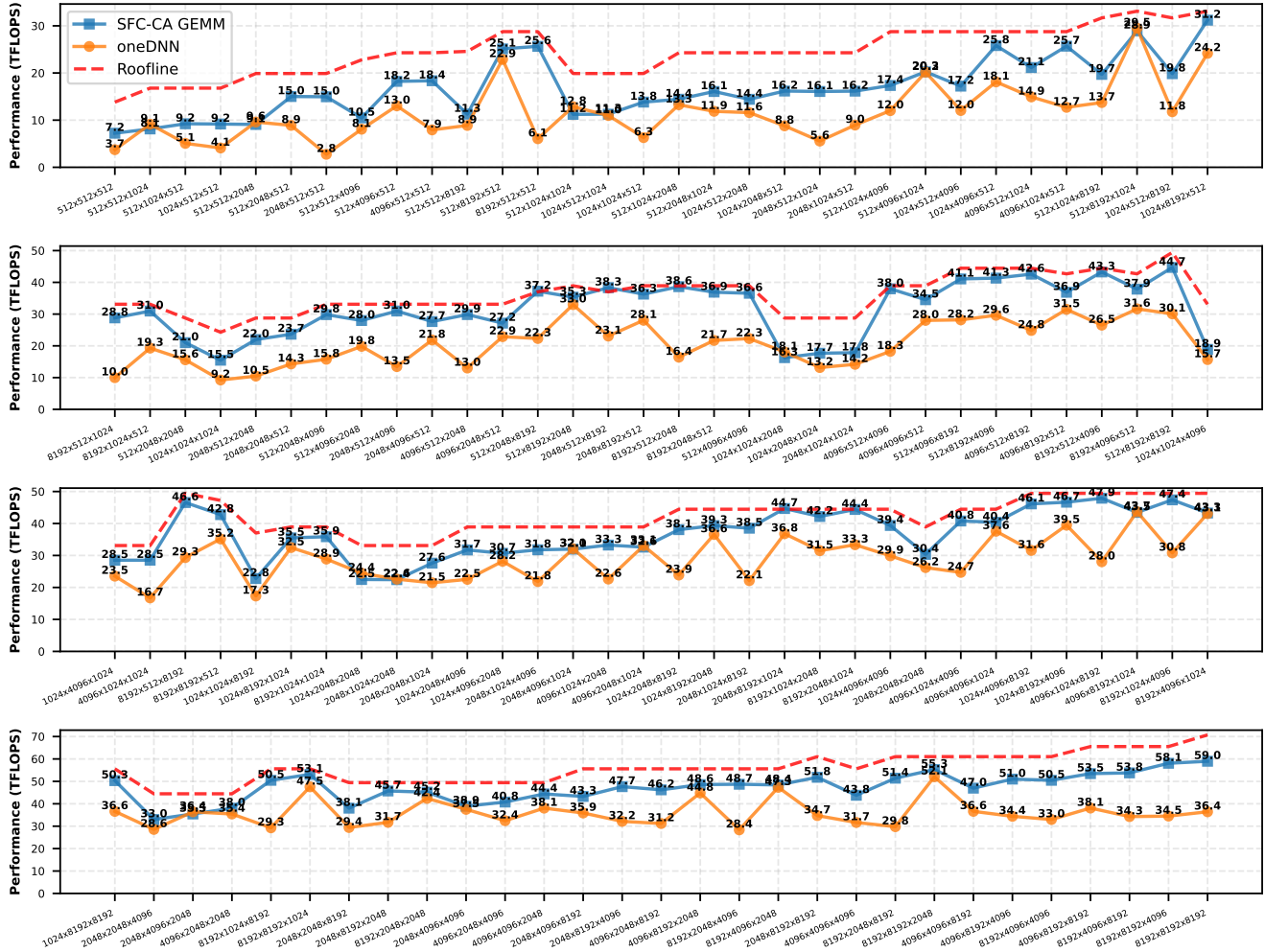


Fig. 5: EMR BF16 GEMM performance for oneDNN and SFC-CA GEMM for a range of matrices ( $M \times N \times K$  configuration illustrated on x-axis), along with the roofline performance as projected by the model described in Section II-F. The y-axis shows achieved BF16 TFLOPS. The experiments are sorted based on their operational intensity.

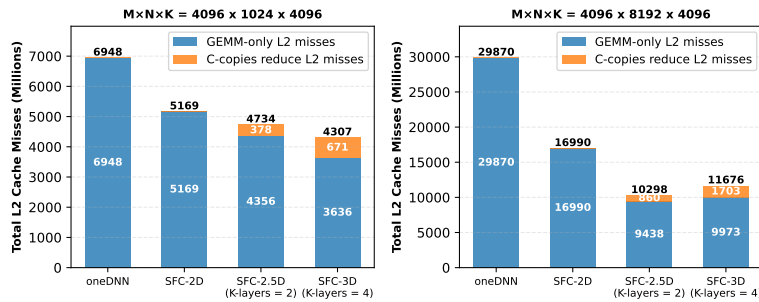


Fig. 6: Total L2 misses on EMR for two problem sizes.

**5th Gen AMD EPYC (ZEN5):** A 5th Gen AMD EPYC server with 96 cores (via an AWS bare metal m8a.metal-24x1 instance). The Bfloat16 matrix multiplication can be accelerated via AVX512 BF16 FMA instructions.

**Graviton 4 (GVT4):** A 4th generation AWS Graviton server with 96 cores (via an AWS bare metal r8g.metal-24x1 in-

stance). The GVT4 ISA (Instruction Set Architecture) is based on Armv9.0-A, featuring high-performance Arm Neoverse-V2 cores. The Bfloat16 matrix multiplication can be accelerated via the BFMMLA instructions [21].

We experimented with a range of 125 matrix shapes (cross product of dimensions  $M$ ,  $N$  and  $K$  from the set  $\{512, 1024, 2048, 4096, 8192\}$ ) which exhibit various aspect ratios for the matrices  $A$ ,  $B$  and  $C$ . With respect to vendor-optimized libraries, we used the SOTA library oneDNN [26] for the x86 platforms (EMR/GNR/ZEN5). For the Arm platform (GVT4) we used the optimized Arm Compute Library (ACL) [27] via the oneDNN frontend. In all GEMM cases, we benchmarked a set of  $A/B/C$  matrices with each set having a proper cardinality to ensure that each GEMM gets the input tensors from memory (i.e. “cold” tensors), and we repeated each experiment 10 times (we report the average performance for each experiment). For the SFC-CA GEMM we experimented with a varying number of replication factors

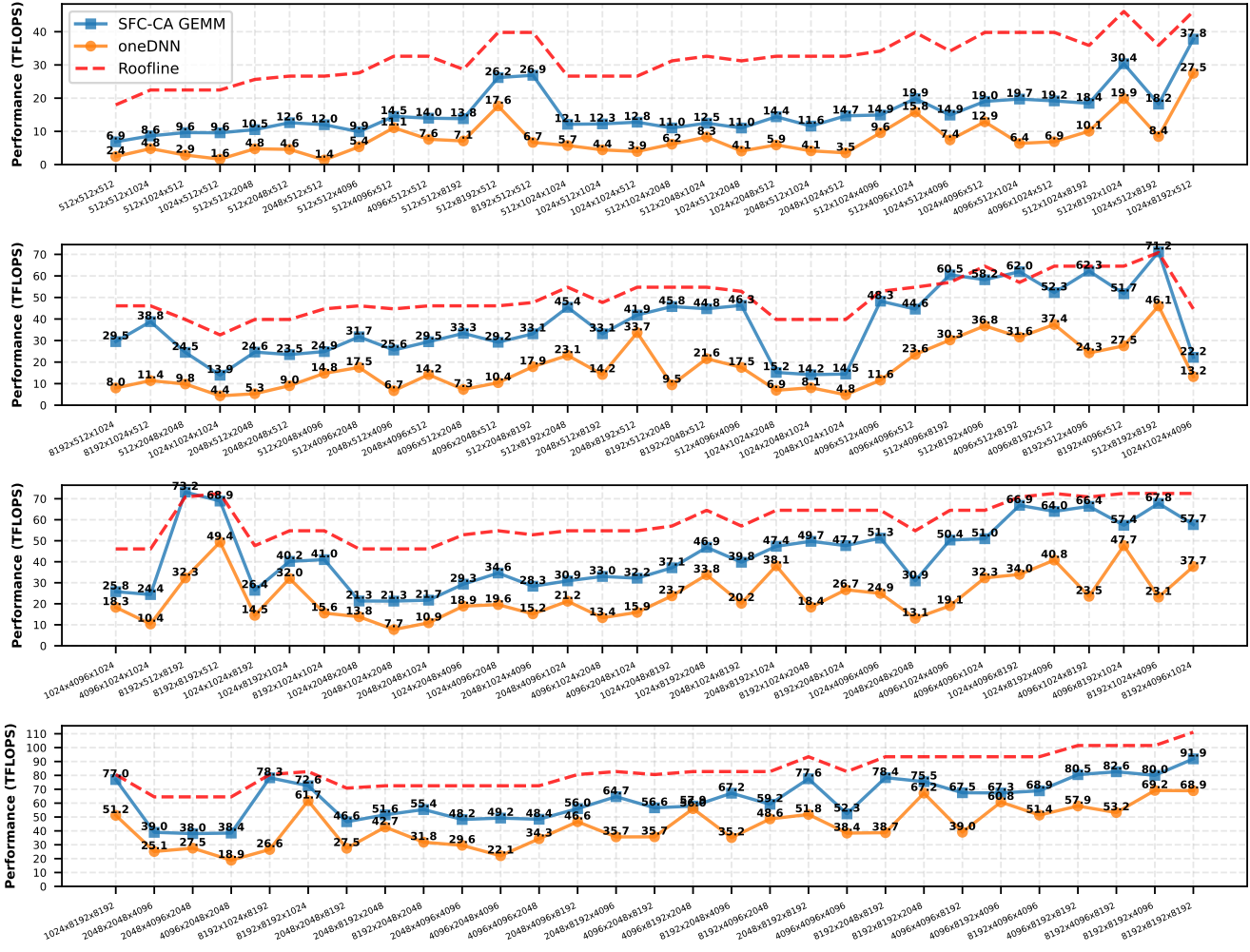


Fig. 7: GNR BF16 GEMM performance for oneDNN and SFC-CA GEMM for a range of  $M \times N \times K$  configurations.

$\{1, 2, 4\}$  and  $K$  block factors  $\{1, 2, 4, 8\}$  and we report the configuration that yields the best performance. Finally, for the roofline models we extracted the  $\beta$  and  $\gamma$  factors for each CPU platform via the corresponding microbenchmarks from LIBXSMM [28] and ArchBench suite [24]. For all the GEMM experiments we used the Bfloat16 (BF16) precision [29] for all the involved tensors in order to leverage the Matrix Multiplication Acceleration instructions on the aforementioned platforms, even though (as mentioned in Section II-G) the precision/datatype of SFC-CA GEMM may be parameterized and is oblivious to the implementation.

### B. Experimental results

Figure 5 illustrates the BF16 GEMM performance for oneDNN and SFC-CA GEMM on EMR for a range of matrices ( $M \times N \times K$  configuration illustrated on x-axis), along with the roofline performance as projected by the model described in Section II-F. The experiments are sorted based on their operational intensity (defined as the total GEMM floating point operations divided by the total size of  $A$ ,  $B$  and  $C$ ).

First we observe that oneDNN illustrates performance far-off the roofline model and shows substantial ‘‘glass-jaws’’. SFC-CA GEMM substantially improves performance by  $1.4 \times$  (geometric mean speedup) and tracks the roofline closely (typically within 5-15% of the tight roofline).

In order to shed light on the source of the performance improvements, we investigated the total L2 misses across all cores for 2 different GEMM experiments – see Figure 6. For the first configuration ( $M \times N \times K = 4096 \times 1024 \times 4096$ , Figure 6-Left), we first observe that the SFC-CA 2D (i.e. 1  $C$  copy) results in total  $1.34 \times$  less L2 misses than oneDNN. By increasing the replication factor to 2 (i.e. 2.5D SFC-CA) we further reduce the total L2 misses by  $1.18 \times$  in the GEMM phase (see blue bars) while we incur some additional L2 misses during the  $C$  reduction (orange part of the bar). Finally, by increasing the replication factor to 4 (i.e. 3D SFC-CA) we further reduce the total L2 misses by  $1.2 \times$  in the GEMM phase while we incur extra L2 misses during the  $C$  reduction phase (which is now  $\sim 2 \times$  larger compared to the case with just 2  $C$  copies). Nevertheless, the 3D SFC-CA GEMM with 4 copies

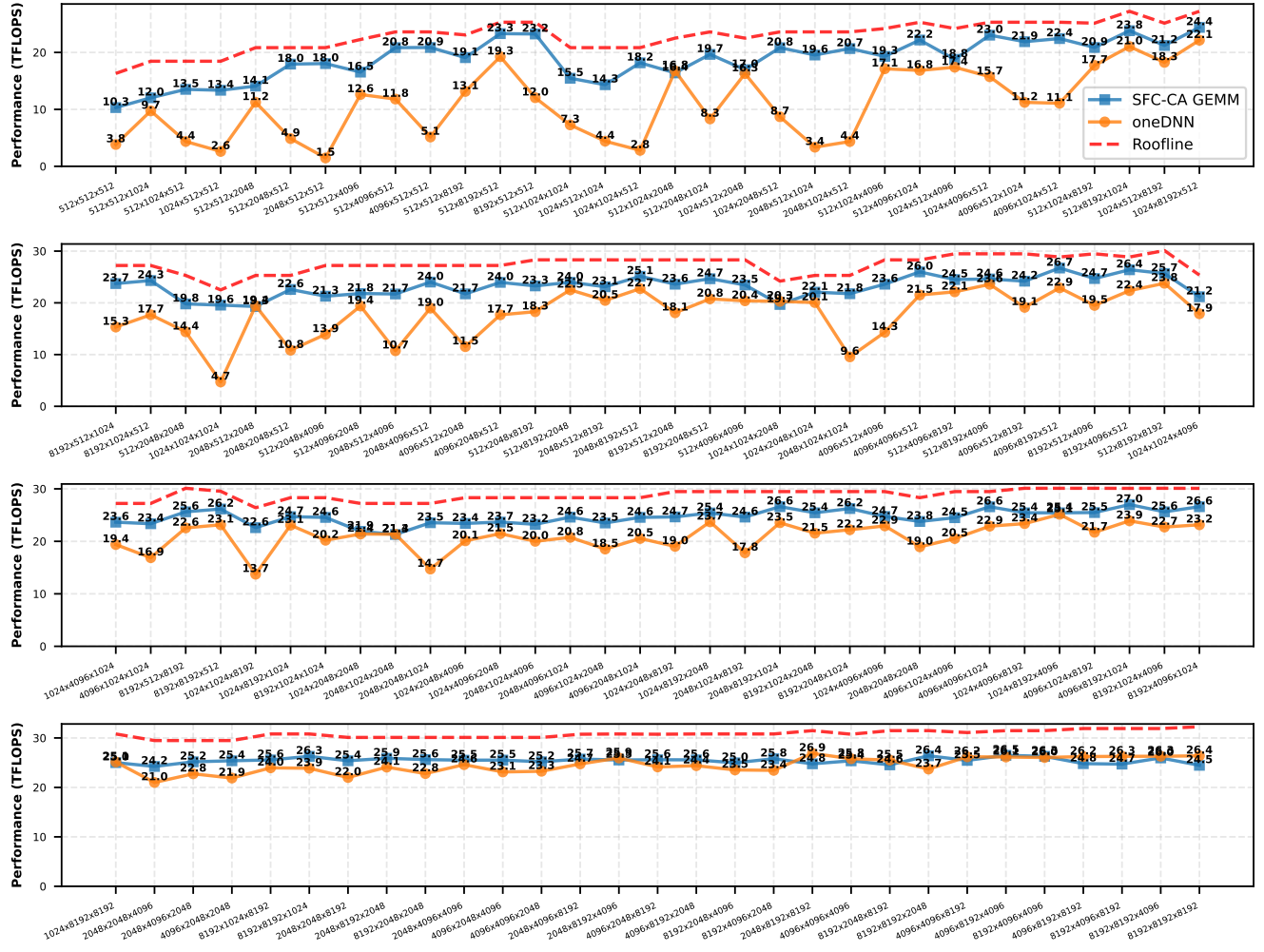


Fig. 8: ZEN5 BF16 GEMM performance for oneDNN and SFC-CA GEMM for a range of  $M \times N \times K$  configurations.

of  $C$  is the best performing variant in this case, yielding in total  $1.61 \times$  less L2 cache misses than the oneDNN implementation. For this specific experiment we observe that SFC-CA GEMM is  $1.65 \times$  faster than oneDNN (40.8 vs 24.7 TFLOPs).

For the second configuration ( $M \times N \times K = 4096 \times 8192 \times 4096$ , Figure 6-Right) we derive the same conclusions. The best performing SFC-CA GEMM in this case corresponds to the case with 2  $C$  copies (2.5D SFC-CA) and results in total reduction of L2 misses by  $2.9 \times$  compared to oneDNN. For this experiment we observe that SFC-CA GEMM is  $1.5 \times$  faster than oneDNN (51 vs 34.4 TFLOPs). These experimental results also show the importance of tuning the replication factor in order to balance the benefits on reduced data-movement in the GEMM phase and the additional overhead due to the reduction of the  $C$  copies which increases as the number of  $C$  copies rises. Even though we illustrated the total L2 misses as a Figure of Merit to explain the observed performance, it is noteworthy that not all L2 misses have equal impact on the final performance. For example, excessive L2 misses pertaining to  $A/B$  accesses within the BRGEMM

invocations (i.e. in the blue parts of the bars) may cause stalls in the pipeline and subsequently prevent the out-of-order execution of the fused-multiply-add (FMA) instructions (either they are traditional vector FMAs or Tile Matrix Multiplication instructions like AMX). On the other hand, L2 misses in streaming kernels like the final reduction of  $C$  copies have less impact on the latency.

Figure 7 illustrates the BF16 GEMM performance for oneDNN and SFC-CA Algorithm for the same range of matrices on GNR. Again we observe that SFC-CA GEMM substantially outperforms oneDNN by  $2 \times$  (geometric mean speedup) and tracks the roofline closely (typically within 5-25% of the tight roofline for the GEMM shapes with larger operational intensity, i.e. last two plots).

Figure 8 exhibits the BF16 GEMM performance for oneDNN and SFC-CA Algorithm on ZEN5. SFC-CA GEMM outperforms oneDNN by  $1.4 \times$  (geometric mean speedup) and tracks the roofline closely (typically within 5-10%).

Last, Figure 9 exhibits the BF16 GEMM performance for the arm-optimized ACL library (via the oneDNN frontend)

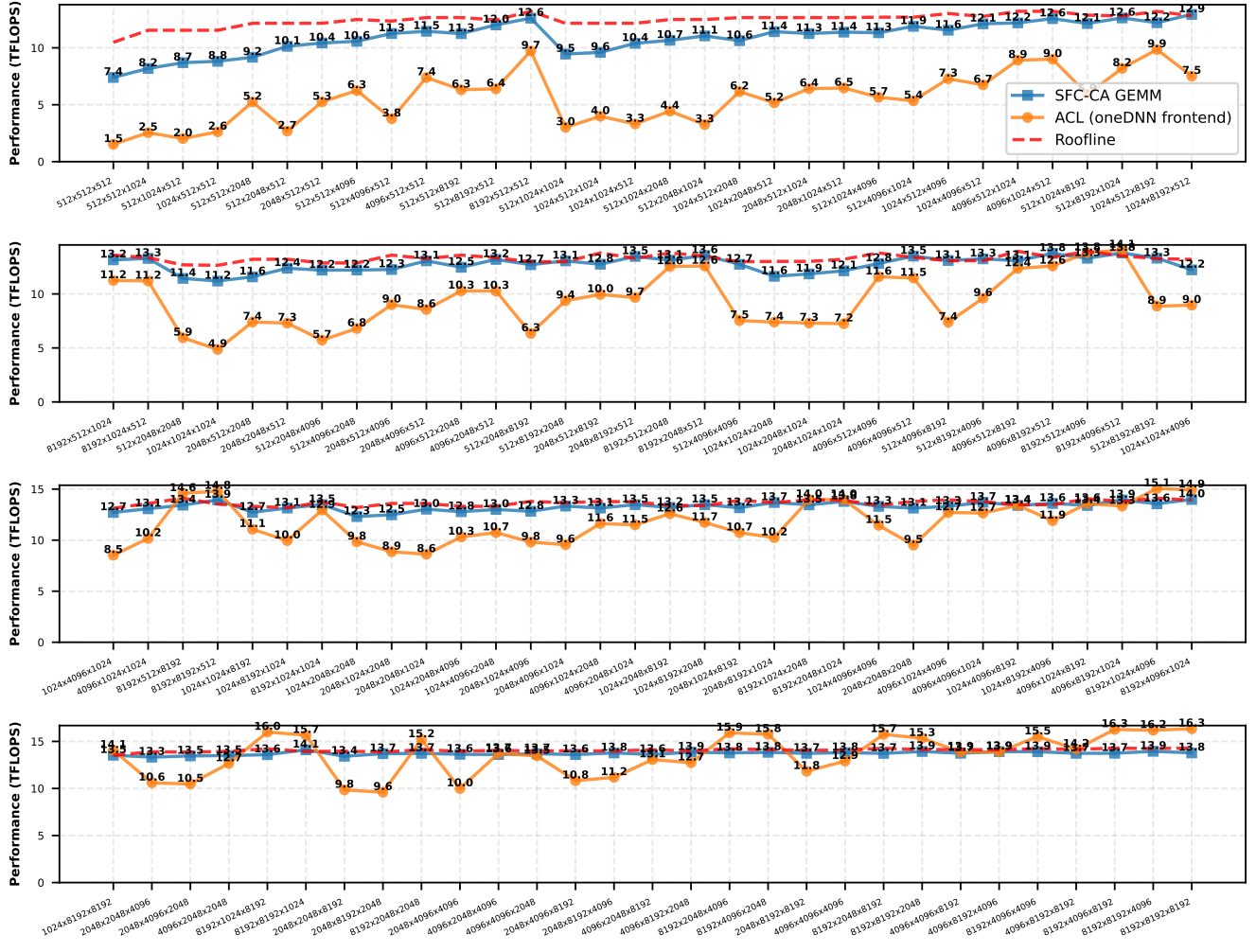


Fig. 9: GVT4 BF16 GEMM for ACL (via the oneDNN frontend) and SFC-CA GEMM for a range of  $M \times N \times K$  configurations.

and SFC-CA GEMM on GVT4. SFC-CA GEMM outperforms ACL by  $1.4\times$  (geometric mean speedup) and tracks the roofline closely (typically within 5% of the tight roofline). We note here that our roofline is derived by benchmarking the LIBXSMM BRGEMM in order to extract the  $\gamma$  model parameter (see Section II-F). However, for some cases the ACL GEMM microkernel is outperforming the corresponding one in LIBXSMM and as a result the eventual ACL performance is slightly higher than the roofline. Our hypothesis is that ACL formats the  $B$  matrix in a layout that favors the BFMMMA instruction (it requires  $B$  matrix to be transposed) and therefore achieves higher throughput, whereas the LIBXSMM microkernel transposes the  $B$  matrix on the fly, incurring some performance penalty in the single-core BRGEMM microkernel.

All in all, we conclude that the SFC-CA GEMM Algorithm outperforms the vendor-optimized libraries across the board, in a platform-portable way. Note that the Listing 1 does *not* include any platform-specific tuning knobs pertaining to the number of cores, memory hierarchy, cache-sizes etc.

#### IV. RELATED WORK

Communication Avoiding GEMM algorithms have been explored mostly in the context of distributed memory systems, yielding substantial speedups [17]–[19], [30]. The CARMA algorithm [19] is a recursive matrix multiplication algorithm that is communication optimal and the corresponding work includes some shared memory results, however the performance upside over vendor-optimized libraries is limited and mainly originates from GEMM shapes that look like “inner-products”; the authors claim that the benefits in the shared memory case are primarily due to the local matrix multiplications being close to square. Prior work [16], [31] has also explored SFC in order to accelerate the GEMM operations, however it uses the SFC as a tool to derive locality-friendly tensor layouts, but fails to generalize, yields complicated indexing in the GEMM micro-kernels and eventually offers limited performance upside over vendor-optimized libraries. To the best of our knowledge, SFC-CA GEMM (this work) is the first GEMM algorithm that seamlessly integrates the locality-preserving properties of SFC and the communication-avoiding

techniques to provably minimize the data-movement on the critical path and maximize the GEMM throughput, in a performance-portable way and without the need for specialized tensor layouts.

The de-facto standard for obtaining SOTA GEMM performance on modern platforms is using vendor-optimized libraries like oneDNN [26] and ACL [27]. However, as we illustrated in this work, these library approaches typically show performance “glass jaws” which is a direct artifact of the intricacies of modern platforms with matrix multiplication acceleration engines. These matrix multiplication accelerators make data movement (and minimization thereof) essential in order to maximize performance since they skew the FLOP/byte balance of modern CPU platforms. As a result, the optimal exhaustive auto-tuning of libraries is practically infeasible, leading eventually to suboptimal performance.

Tensor compilers with auto-tuning support (e.g. [32]–[35]) offer an alternative to the GEMM libraries. Such frameworks treat tensors as first-class objects, and provide optimizations targeting GEMMs (e.g. polyhedral optimizations for data movement). However, compilers struggle to optimize the GEMM-flavored loop nests for the nuances of the increasingly complex architectures. Our work can be seen as complementary to this effort, where the GEMM-flavored loops are tackled with SFC and the Communication Avoiding techniques in a shape-oblivious and platform-oblivious fashion. Due to the simplicity of SFC-CA GEMM and its platform-agnostic nature, it may serve as a robust tensor contraction framework within Tensor Compilers, obviating the need for complicated cache locality analysis/optimizations and parallelization orchestration.

## V. CONCLUSIONS AND FUTURE WORK

In this work we presented SFC-CA GEMM, a Space Filling Curve based GEMM that seamlessly implements a class of provably-optimal communication avoiding matrix multiplication algorithms. SFC-CA GEMM is compact ( $\sim 30$  LOC), yet it achieves state-of-the-art (SOTA) results on multiple CPU platforms, outperforming vendor libraries by up to  $2\times$  (geometric-mean speedup) for a range of GEMM shapes. Even though we described SFC-CA GEMM in the context of multi-core CPUs, the same methodology with SFC-based partitioning and tensor replication can be applied to GPU GEMM algorithms to reduce the data-movement across the memory hierarchy. Due to its simplicity and platform-agnostic nature, the SFC-CA GEMM may also serve as a robust tensor contraction framework within Tensor Compilers, obviating the need for complicated cache locality analysis/optimizations and parallelization orchestration. Last but not least, the same SFC-based contraction methodology readily extends to higher dimensions. For example, one can implement convolutions by mapping the 3D index space of the output tensor into an 1D SFC-index by using Hilbert curves of higher dimensionality.

## REFERENCES

- [1] Alex Krizhevsky, I. Sutskever, and G.E. Hinton. Image classification with deep convolutional neural networks. *Advances in neural information processing systems*, pages 1097–1105, 2012.
- [2] Christian Szegedy, Wei Liu, Yangqing Jia, Pierre Sermanet, Scott Reed, Dragomir Anguelov, Dumitru Erhan, Vincent Vanhoucke, and Andrew Rabinovich. Going deeper with convolutions. In *Proceedings of the IEEE conference on computer vision and pattern recognition*, pages 1–9, 2015.
- [3] Karen Simonyan and Andrew Zisserman. Very deep convolutional networks for large-scale image recognition. *arXiv preprint arXiv:1409.1556*, 2014.
- [4] Dong Yu, Michael L Seltzer, Jinyu Li, Jui-Ting Huang, and Frank Seide. Feature learning in deep neural networks—studies on speech recognition tasks. *arXiv preprint arXiv:1301.3605*, 2013.
- [5] Yonghui Wu, Mike Schuster, Zhifeng Chen, Quoc V Le, Mohammad Norouzi, Wolfgang Macherey, Maxim Krikun, Yuan Cao, Qin Gao, Klaus Macherey, et al. Google’s neural machine translation system: Bridging the gap between human and machine translation. *arXiv preprint arXiv:1609.08144*, 2016.
- [6] Heng-Tze Cheng, Levent Koc, Jeremiah Harmsen, Tal Shaked, Tushar Chandra, Hrishi Aradhye, Glen Anderson, Greg Corrado, Wei Chai, Mustafa Ispir, et al. Wide & deep learning for recommender systems. In *Proceedings of the 1st Workshop on Deep Learning for Recommender Systems*, pages 7–10. ACM, 2016.
- [7] Thomas Wolf, Julien Chaumond, Lysandre Debut, Victor Sanh, Clement Delangue, Anthony Moi, Pierrick Cistac, Morgan Funtowicz, Joe Davison, Sam Shleifer, et al. Transformers: State-of-the-art natural language processing. In *Proceedings of the 2020 Conference on Empirical Methods in Natural Language Processing: System Demonstrations*, pages 38–45, 2020.
- [8] Erik Gawehn, Jan A Hiss, and Gisbert Schneider. Deep learning in drug discovery. *Molecular informatics*, 35(1):3–14, 2016.
- [9] Garrett B Goh, Nathan O Hadas, and Abhinav Vishnu. Deep learning for computational chemistry. *Journal of computational chemistry*, 38(16):1291–1307, 2017.
- [10] Maithra Raghu and Eric Schmidt. A survey of deep learning for scientific discovery. *arXiv preprint arXiv:2003.11755*, 2020.
- [11] Edoardo Angelo Di Napoli, Paolo Bientinesi, Jiajia Li, and André Uschmajew. High-performance tensor computations in scientific computing and data science. *Frontiers in Applied Mathematics and Statistics*, page 93, 2022.
- [12] Evangelos Georganas, Dhiraj Kalamkar, Sasikanth Avancha, Menachem Adelman, Cristina Anderson, Alexander Breuer, Jeremy Bruestle, Narendra Chaudhary, Abhisek Kundu, Denise Kutnick, et al. Tensor processing primitives: A programming abstraction for efficiency and portability in deep learning workloads. In *Proceedings of the International Conference for High Performance Computing, Networking, Storage and Analysis*, pages 1–14, 2021.
- [13] Evangelos Georganas, Dhiraj Kalamkar, Kirill Voronin, Abhisek Kundu, Antonio Noack, Hans Pabst, Alexander Breuer, and Alexander Heinecke. Harnessing deep learning and hpc kernels via high-level loop and tensor abstractions on cpu architectures. In *2024 IEEE International Parallel and Distributed Processing Symposium (IPDPS)*, pages 950–963. IEEE, 2024.
- [14] Evangelos Georganas, Kunal Banerjee, Dhiraj Kalamkar, Sasikanth Avancha, Anand Venkat, Michael Anderson, Greg Henry, Hans Pabst, and Alexander Heinecke. Harnessing deep learning via a single building block. In *2020 IEEE International Parallel and Distributed Processing Symposium (IPDPS)*, pages 222–233. IEEE, 2020.
- [15] Jakub Červený. Gilbert. <https://github.com/jakubcerveny/gilbert>, 2019.
- [16] Alexander Heinecke and Michael Bader. Parallel matrix multiplication based on space-filling curves on shared memory multicore platforms. In *Proceedings of the 2008 workshop on Memory access on future processors: a solved problem?*, pages 385–392, 2008.
- [17] Edgar Solomonik and James Demmel. Communication-optimal parallel 2.5 d matrix multiplication and lu factorization algorithms. In *European Conference on Parallel Processing*, pages 90–109. Springer, 2011.
- [18] Evangelos Georganas, Jorge González-Domínguez, Edgar Solomonik, Yili Zheng, Juan Tourino, and Katherine Yelick. Communication avoiding and overlapping for numerical linear algebra. In *SC’12: Proceedings of the International Conference on High Performance Computing, Networking, Storage and Analysis*, pages 1–11. IEEE, 2012.

[19] James Demmel, David Eliahu, Armando Fox, Shoaib Kamil, Benjamin Lipshitz, Oded Schwartz, and Omer Spillinger. Communication-optimal parallel recursive rectangular matrix multiplication. In *2013 IEEE 27th International Symposium on Parallel and Distributed Processing*, pages 261–272. IEEE, 2013.

[20] Martin D Schatz, Jack Poulson, and Robert A van de Geijn. Scalable universal matrix multiplication algorithms: 2d and 3d variations on a theme. *submitted to ACM Transactions on Mathematical Software*, pages 1–30, 2012.

[21] Evangelos Georganas, Dhiraj Kalamkar, Kirill Voronin, Abhisek Kundu, Antonio Noack, Hans Pabst, Alexander Breuer, and Alexander Heinecke. Harnessing deep learning and hpc kernels via high-level loop and tensor abstractions on cpu architectures. In *2024 IEEE International Parallel and Distributed Processing Symposium (IPDPS)*, pages 950–963. IEEE, 2024.

[22] Samuel Williams, Andrew Waterman, and David Patterson. Roofline: an insightful visual performance model for multicore architectures. *Communications of the ACM*, 52(4):65–76, 2009.

[23] Alexander Heinecke, Greg Henry, Maxwell Hutchinson, and Hans Pabst. Libxsmm: accelerating small matrix multiplications by runtime code generation. In *SC’16: Proceedings of the International Conference for High Performance Computing, Networking, Storage and Analysis*, pages 981–991. IEEE, 2016.

[24] Alexander Heinecke. archbench. <https://github.com/alheinecke/ArchBenchSuite>, 2026.

[25] Intel Architecture Instruction Set Extensions and Future Features Programming Reference. <https://www.intel.com/content/www/us/en/content-details/671368/intel-architecture-instruction-set-extensions-programming-reference.html>, Accessed on 1/21/2026.

[26] Intel oneDNN. <https://github.com/oneapi-src/onednn>, Accessed on 4/6/2023.

[27] ARM. <https://github.com/arm-software/computelibrary>, Accessed on 4/6/2023.

[28] Alexander Heinecke, Greg Henry, Maxwell Hutchinson, and Hans Pabst. LIBXSMM: Accelerating small matrix multiplications by runtime code generation. In *Proceedings of the International Conference for High Performance Computing, Networking, Storage and Analysis, SC ’16*, pages 84:1–84:11, Piscataway, NJ, USA, 2016. IEEE Press.

[29] “Using bfloat16 with TensorFlow models”. <https://cloud.google.com/tpu/docs/bfloat16>, Accessed on 4/3/2019.

[30] Grzegorz Kwasniewski, Marko Kabić, Maciej Besta, Joost VandeVondele, Raffaele Solca, and Torsten Hoefer. Red-blue pebbling revisited: near optimal parallel matrix-matrix multiplication. In *Proceedings of the International Conference for High Performance Computing, Networking, Storage and Analysis*, pages 1–22, 2019.

[31] Nico Reissman, Jan Christian Meyer, and Magnus Jähre. A study of energy and locality effects using space-filling curves. In *2014 IEEE International Parallel & Distributed Processing Symposium Workshops*, pages 815–822. IEEE, 2014.

[32] Tianqi Chen, Thierry Moreau, Ziheng Jiang, Lianmin Zheng, Eddie Yan, Haichen Shen, Meghan Cowan, Leyuan Wang, Yuwei Hu, Luis Ceze, et al. {TVM}: An automated end-to-end optimizing compiler for deep learning. In *13th {USENIX} Symposium on Operating Systems Design and Implementation ({OSDI} 18)*, pages 578–594, 2018.

[33] Nicolas Vasilache, Oleksandr Zinenko, Theodoros Theodoridis, Priya Goyal, Zachary DeVito, William S Moses, Sven Verdoolaege, Andrew Adams, and Albert Cohen. Tensor comprehensions: Framework-agnostic high-performance machine learning abstractions. *arXiv preprint arXiv:1802.04730*, 2018.

[34] Fredrik Kjolstad, Stephen Chou, David Lugato, Shoaib Kamil, and Saman Amarasinghe. Taco: A tool to generate tensor algebra kernels. In *2017 32nd IEEE/ACM International Conference on Automated Software Engineering (ASE)*, pages 943–948. IEEE, 2017.

[35] Jianhui Li, Zhennan Qin, Yijie Mei, Jingze Cui, Yunfei Song, Ciyong Chen, Yifei Zhang, Longsheng Du, Xianhang Cheng, Baihui Jin, et al. onednn graph compiler: A hybrid approach for high-performance deep learning compilation. In *2024 IEEE/ACM International Symposium on Code Generation and Optimization (CGO)*, pages 460–470. IEEE, 2024.

the results to vary. You should consult other information and performance tests to assist you in fully evaluating your contemplated purchases, including the performance of that product when combined with other products. For more information go to <http://www.intel.com/performance>. Intel, Xeon, and Intel Xeon Phi are trademarks of Intel Corporation in the U.S. and/or other countries.